Reply to Yuichi Otsuka and Referee #1

(1) : Reply to Yuichi Otsuka

This paper reports all-sky airglow and GNSS-TEC observations of plasma bubbles growing around sunrise terminator during a magnetic storm. This work could contribute to study of effects of magnetic storm on ionospheric disturbances. Therefore, this paper is worth publishing in this journal. However, the followings need to be addressed before its publication.

Reply: Thank you for your positive comments. All the comments from you have been considered in the revised manuscript. And with the corrections made, we hope it's accepted for publication in Annales Geophysicae now.

Specific comments: – "recombination": This reviewer recommends the authors to use a term "merging". "Recombination" is confusing because "recombination" is widely used to represent reaction of ions with electrons resulting in neutralization. "Merging" is used commonly compared to "recombination". See the following references:

Narayanan, V. L., S. Gurubaran, and K. Shiokawa (2016), Direct observational evidence for the merging of equatorial plasma bubbles, J. Geophys. Res. Space Physics,121, 7923–7931, doi:10.1002/2016JA022861.
Huba, J. D., T.-W. Wu, and J. J. Makela (2015), Electrostatic reconnection in the ionosphere, Geophys. Res. Lett., 42, 1626–1631, doi:10.1002/2015GL063187.
Huang, C.-S., J. M. Retterer, O. de La Beaujardiere, P. A. Roddy, D. E. Hunton, J. O. Ballenthin, and R. F. Pfaff (2012), Observations and simulations of formation of broad plasma depletions through merging process, J. Geophys. Res., 117, A02314, doi:10.1029/2011JA017084.- l.

Reply**:** Thanks for this suggestion. After reading above references, we used "merging" to replace "recombination" and cited those references in the revised manuscript.

- l. 55, "and the background ionospheric/thermosphere": Describe concretely which parameter the authors mean. Does the authors mean vertical gradient of plasma density at the bottomside of the F region or ion-neutral collision frequency?

Reply: We want to address that the growth rate of Rayleigh-Taylor instability (RTI) will be influenced by the vertical gradient of plasma density at the bottomside of F region, and also the change of ion-neutral collision frequency. We have revised related texts at lines 55-56.

- l. 96, "Hall electric field": It is better to add more detailed explanation of the Hall electric field.

Reply: In the revised manuscript, we added related explanation of "Hall electric field" at lines 95-99.
"Santos et al. (2016) also showed some EPBs of zonal drifts reversal (eastward to westward) during a geomagnetic storm, and they suggested the reversal was caused by a vertical Hall electric field which induced by a zonal prompt penetration electric field (PPEF) in the presence of enhanced conductivity in the E region during night."

Santos, A. M., Abdu, M. A., Souza, J. R., Sobral, J. H. A., Batista, I. S., and Denardini, C. M.: Storm time equatorial plasma bubble zonal drift reversal due to disturbance Hall electric field over the Brazilian region, J. Geophys. Res., 121, 5594–5612, https://doi.org/10.1002/2015JA022179, 2016.

– ll. 110-111, Figure 1: Field-of-view (FOV) is shown by a circle in Figure 1. It would be better to describe the zenith angle corresponding to the circle shown as

FOV.

Reply: In Figure 1, the blue circle represents the projected regions with a radius of ~900 km [about 140° field of view (FOV)] of the all-sky imager at an altitude of 250 km. We have revised related texts at lines 113-115.

– l. 122: Describe minimum and maximum frequency (or period) of the band-pass filter.

Reply: The minimum and maximum period of the band-pass filters we used are 2 min and 12 min, respectively. In the revised manuscript, we added related content at lines 126-127.

– ll. 176-197: The authors describe that TEC depletion can be seen in Figures 4 and 5. However, TEC variations in these figures show positive and negative values rather than depletion. Spatial scale of the TEC variations seen in the figures is small. Therefore, the TEC variation corresponds to the plasma density irregularities existing within plasma bubbles. If the authors show ROTI (Rate of TEC change Index), structure of the plasma bubbles can be seen clearly as ROTI enhancements. See the following paper.
Buhari, S. M., Abdullah, M., Hasbi, A. M., Otsuka, Y., Yokoyama, T., Nishioka, M., and Tsugawa, T. (2015), Continuous generation and twoâĂ˘ Rdimensional structure of equatorial plasmabubbles observed by highâĂ˘ Rdensity GPS receivers in Southeast Asia, J. Geophys. Res. Space Physics, 119, pages 10,569– 10,580.doi:10.1002/2014JA020433.

Reply: Thanks for your advice. We calculated the ROTI variations (Figure 6) which correspond geographical area and time of each airglow imaging in the revised manuscript. In the Figure 6, we can clearly ROTI enhancement from structure of the EPBs.
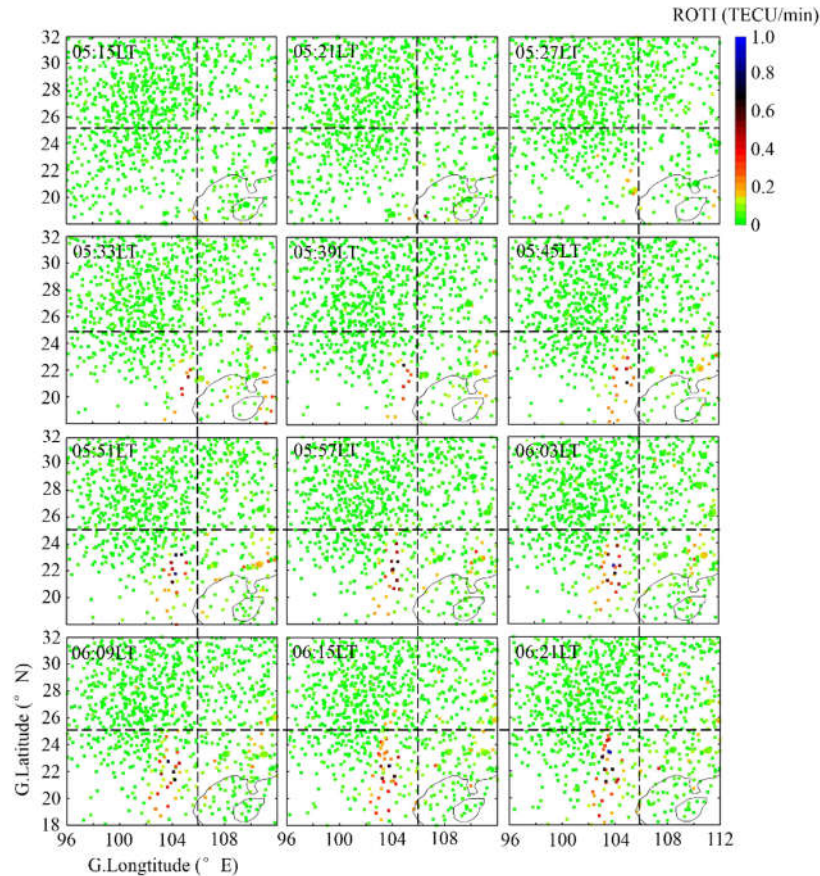
Figure 6. Two-dimensional map of rate of TEC index (ROTI) correspond to each image of Figure 3. The black horizontal line is a reference line of 25° N. The black vertical line is a reference line of 106° E.

– ll. 229-232: **Explain a reason why the eastern wall of EPB is unstable when the wind blows westward and equatorward. When the wind blow westward, and thus the wind-induced Pedersen current flows downward, gradient-drift instability can occur at the eastern wall of EPB, where the plasma density gradient is eastward. On the other hand, how does the equator ward wind work?**

Reply: Due to Coriolis force, the enhanced equatorward wind at disturbed periods will have also a westward component, which will work on the eastward wall of EPB, causing the secondary instabilities. Similar finding of secondary instability happened at the eastward wall of EPB has been earlier reported by Makela et al. (2006), by using airglow imagers. In the revised manuscript, we added related context at lines 251-256.

Makela, J. J., Kelley, M. C., and Nicolls, M. J.: Optical observations of the development of secondary instabilities on the eastern wall of an equatorial plasma bubble J. Geophys. Res., 111, A9, https://doi.org/10.1029/2006JA011646, 2006.

– ll. 233-247, "This is because zonal drift value of EPBs ... EPBs should be influenced by ionospheric electric field.": The authors point out that the drift velocity of EPB is smaller than the wind, and argue the reason of this difference. However, this reviewer cannot understand what the authors are describing. If the F-region dynamo process completely works, the ExB drift velocity is equal to the wind velocity. Does the authors mean that electric field generation through the F-region dynamo is not completed and thus the ExB drift is smaller than the wind velocity? Otherwise, does the authors consider another electric field, which is different from the dynamo electric filed induced by the wind?

Reply: Here, our understanding is that the zonal plasma drifts are affected by the vertical electric fields generated by the E and F region wind dynamo (Haerendel et al., 1992). The E and F region dynamo effects can be examined by using a simplified formula from Eccles et al. (1998): $V_\varphi = U_\varphi^P = \frac{\Sigma_P^F U_\varphi^{PF} + \Sigma_P^E U_\varphi^{PE}}{\Sigma_P}$. Where V_φ is the zonal plasma drift speed, U_φ^P is the Pedersen conductivity-weighted neutral zonal winds, Σ is the field-line-integrated total ionospheric conductivity. E and F refer to the E and F region, respectively. P represents the Pedersen component. During nighttime, the E layer is quickly recombined and F layer dynamo plays a dominant role. So, the zonal drift value of EPBs should mainly be related to $\frac{\Sigma_P^F U_\varphi^{PF}}{\Sigma_P}$. The simulation of Figure 7 reflect U_φ^{PF}. The difference between the model simulated background zonal winds and the derived zonal drifts of EPBs from airglow images is possibly due to that the model simulation provide mainly reflect a general trend of the wind, but not the exact wind velocity in reality.

Eccles., V. J.: A simple model of low-latitude electric fields, J. Geophys. Res., 103, 26699-26708, https://doi.org/10.1029/98JA02657, 1998.

Haerendel, G., Eccles, J. V., and Çakir, S.: Theory for modeling the equatorial evening ionosphere and the origin of the shear in the horizontal plasma flow, J. Geophys. Res., 97, 1209–1223, https://doi.org/10.1029/91JA02226, 1992.

– ll. 255-256: The authors point out the EPBs kept developing after sunrise. Generally, it is considered that after sunrise, the photoionization due to the Solar EUV radiation produce the plasma in the ionosphere and fill the plasma depletion of EPB. In order to compare the time of sunrise, it would be worth showing local time variation of the absolute TEC, to compare the time of EPB existence with the time of rapid TEC increase at sunrise.

Reply: In the revised manuscript, we added it in Figure 5. The TEC depletions showed that EPBs existed after sunrise and they disappeared after 07:45 LT. These results showed that they vanished about one hour after sunrise. Their life time lasted for at least about 3 hours.

– l. 265, "during the development phase of storm": What is the development phase of storm? Is it "main phase of magnetic storm"? Why does the DDEF appear only during the development phase of storm?

Reply: We are sorry for the misleading description in our previous manuscript. Once DDEF established, the DDEF could be last from hours to couple of days (Richmond et al., 2003). So, we rewrote the sentence in the revised manuscript. It is modified for "The DDEF caused by storm will drive plasma drift to move upward during nighttime (Blanc and Richmond, 1980)".

Blanc, M., and Richmond, A. D.: The ionospheric disturbance dynamo, J. Geophys. Res., 85, A4, https://doi.org/10.1029/JA085iA04p01669, 1980.

Richmond, A. D., Peymirat, C., and Roble, R. G.: Long‑lasting disturbances in the equatorial ionospheric electric field simulated with a coupled magnetosphere‑ionosphere‑thermosphere model, J. Geophys. Res., 108, A3, https://doi.org/10.1029/2002JA009758, 2003.

Minor comments:

-l. 127: "Digisond" –> "Digisonde"

-l. 308: "rise" may be "sunrise".

Figure 6: Legend of vertical axis in Figures 6c and 6e is "W-S distance". It should be "W-E distance". Furthermore, describe positive eastward.

Reply: Thank you for these detailed suggestions. We used "Digisonde" to replace "Digisond" and used "sunrise" to replace "rise". The previous Figure 6 has been updated as Figure 7 in the revision.
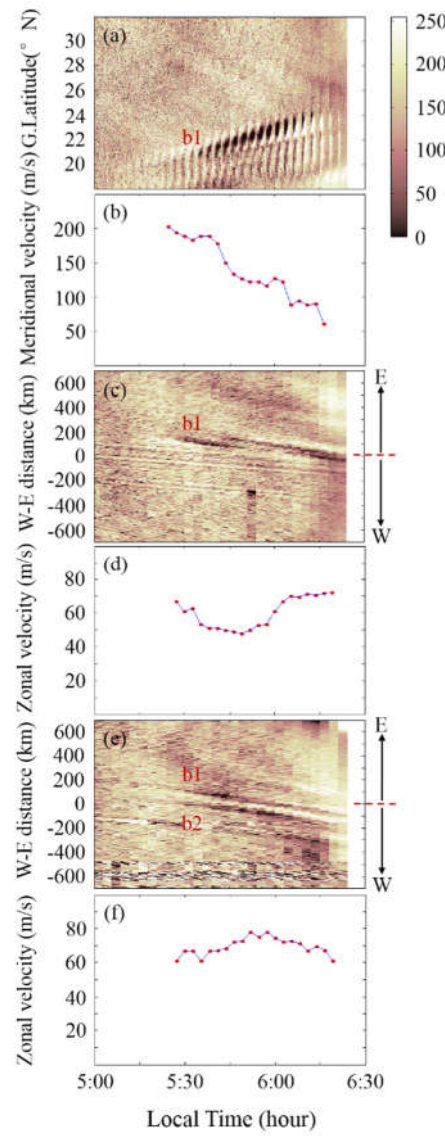
Figure 7. (a) N-S cross sections (between 104°E and 105°E) of the airglow images on 08 November 2015. (c) W-E cross sections (between 21.5°N and 22°N) of the airglow images. (e) W-E cross sections (between 18.5°N and 19°N) of the airglow images. (b) The variations of the meridian velocities of "b1" with local time. (d) and (f) The variations of the zonal velocities of "b1" at ~ 22°N and ~19°N geographical latitudes, respectively.

(2): Reply to Referee #1

This paper reports all-sky airglow and GNSS-TEC observations of plasma bubbles forming around the sunrise terminator during the recovery phase of a magnetic storm. This represents a contribution to the study of magnetic-storm effects on ionospheric disturbances. Therefore, this paper is worth publishing in the journal following minor revision as described below:

Reply: We are grateful to the reviewer for useful comments on our manuscript. All the comments from you and also the other reviewer have been considered in the revised manuscript. And with the corrections made, we hope it's accepted for publication now. Thank you very much!

'Break' and 'recombination' are nonstandard terminology for the phenomena the authors describe; for 'break' people usually say 'bifurcation', and for 'recombination', 'merging'. Actually, the 'break' that appears in the all-sky images looks to me like it could be the development of another bubble, or possibly the emergence of an arm on the side of their main bubble. These phenomena were discussed in detail, with simulations, by Huang et al. (Huang, C.-S., J. M. Retterer, O. de La Beaujardiere, P. A.Roddy, D. E. Hunton, J. O. Ballenthin, and R. F. Pfaff (2012), Observations and simulations of formation of broad plasma depletions through merging process, J. Geophys. Res., 117, A02314, doi:10.1029/2011JA017084.)

Reply: Thanks for your suggestions. After reading your comments and some references, we found it was inappropriate for using 'break' and 'recombination' in the manuscript. So, we used 'bifurcation' and 'merging' to replace 'break' and 'recombination', respectively. Besides, we also cited related reference in the revised manuscript.

The variation of the zonal drift within plasma bubbles with both solar activity and

geomagnetic variations was discussed by Huang and Roddy (Huang, C.-S., and P. A.Roddy (2016), Effects of solar and geomagnetic activities on the zonal drift of equatorial plasma bubbles, J. Geophys. Res. Space Physics, 121, 628–637, doi:10.1002/2015JA021900.), which would be a useful reference here.

Reply: Thanks for your valuable suggestions. After reading the reference, we find the viewpoint of this paper is consistent with our results. It is a very important reference for our manuscript. So, we have cited it in the revised manuscript.

Finally, the presence of bubbles around sunrise was investigated thoroughly in the in-situ observations of the plasma density by the C/NOFS satellite, and those studies should be referenced here: Huang, C.-S., O. de La Beaujardiere, P. A. Roddy, D. E. Hunton, J. O. Ballenthin, and M. R. Hairston (2013),Long-lasting daytime equatorial plasma bubbles observed by the C/NOFS satellite,J. Geophys. Res. Space Physics,118,2398–2408, doi:10.1002/jgra.50252.

Reply: Yes, we keep the same point as yours. Huang et al. (2013) reported the observations of long-lasting daytime EPBs with the C/NOFs satellite during a geomagnetic storm in which the EPBs were persistent from the post-midnight sector through the afternoon. So, we have cited it in the manuscript.

Equatorial Plasma Bubbles Developing Around Sunrise Observed by an All-Sky Imager and GNSS Network during the Storm Time

Kun Wu[1, 2], Jiyao Xu[1, 2], Xinan Yue[3, 2], Chao Xiong[4], Wenbin Wang[6], Wei Yuan[1, 2], Chi Wang[1, 2], Yajun Zhu[5], Ji Luo[1, 2]

[1]State Key Laboratory of Space Weather, National Space Science Center, Chinese Academy of Sciences, Beijing, China

[2]College of Earth and Planetary Sciences, University of Chinese Academy of Sciences, Beijing, China

[3]Key Laboratory of Earth and Planetary Physics, Institute of Geology and Geophysics, Chinese Academy of Sciences, Beijing, China

[4]GFZ German Research Centre for Geosciences, Telegrafenberg, 14473 Potsdam, Germany.

[5]Institute of Energy and Climate Research (IEK-7), Forschungszentrum Juelich GmbH, Juelich, Germany

[6]High Altitude Observatory, National Center for Atmospheric Research, Boulder, CO, USA

Correspondence to: jyxu@spaceweather.ac.cn

1

Manuscript-Tracked Changes

Abstract.

A large number of studies have shown that equatorial plasma bubbles (EPBs) occur mainly after sunset, and they usually drift eastward. However, in this paper, an unusual EPB event was simultaneously observed by an all-sky imager and the Global Navigation Satellite Systems (GNSS) network in southern China, during the recovery phase of geomagnetic storm happened on 6-8 November 2015. Observations from both techniques show that the EPBs appeared near dawn. Interestingly, the observational results show that the EPBs continued to develop after sunrise, and disappeared about one hour after sunrise. The development stage of EPBs lasted for at least about 3 hours. To our knowledge, this is the first time that the evolution of EPBs developing around sunrise was observed by an all-sky imager and the GNSS network. Our observation showed that the EPBs drifted westward, which was different from the usually eastward drifts of post-sunset EPBs. The simulation from TIE-GCM model suggest that the westward drift of EPBs should be related to the enhanced westward winds at storm time. Besides, ~~break~~bifurcation and ~~recombination~~merging processes of EPBs were observed by the all-sky imager in the event. Associated with the development of EPBs, increasing in the ionospheric F region peak height was also observed near sunrise, and we suggest the enhance upward vertical plasma drift during geomagnetic storm plays a major role in triggering the EPBs near sunrise.

The texts of underline represent new contents or changed contents.

The texts of strikethrough indicate that contents have been deleted in the revised manuscript.

1. Introduction

After sunset, plasma density depletions, also called equatorial plasma bubbles (EPBs), sometime occur in the equatorial- and low-latitude ionosphere. A large number of studies have shown that EPBs generally start to develop shortly after sunset during geomagnetic quiet periods (e.g., Weber et al., 1980; Kelley et al., 1986; Xiong et al., 2010; Wu et al., 2018). It is generally believed that the Rayleigh-Taylor instability (RTI) is a plausible mechanism to trigger the EPBs (Kelley, 2009; Makela ~~&~~and Otsuka, 2012). The growth rate of RTI is influenced by a number of different factors, such as the zonal electric field, neutral wind and the ~~background~~

2

56 ~~ionospheric/thermosphere~~ vertical gradient of plasma density at the bottomside of the F

57 region or ion-neutral collision frequency, as well as the strength of magnetic fields (Ott,

58 1978; Abdu, 2001; Burke et al, 2004). The pre-reversal enhancement (PRE) of the

59 eastward electric field around sunset is a main reason for the development of EPBs (e.g.,

60 Fejer et al., 1999; Abdu, 2001; Kelley, 2009; Huang, 2018). Owning to the intensified

61 eastward electric field, near magnetic equator the ionosphere is rapidly elevated to

62 higher altitudes via $E \times B$ drifts, which is favorable for the growth of RTI at the

63 bottomside of the ionosphere.

64 The EPBs are thought to extend along magnetic field lines, and can reach as high as

65 magnetic latitudes of about $\pm 20°$ (Kelley, 2009; Lühr et al., 2014). Xiong et al. (2016,

66 2018) suggest that EPBs have a typical zonal size of about 50 km, by using Swarm in

67 situ electron density measurements as well as ground-based airglow imager. Although

68 the characteristics of EPBs have been widely studied, special events, especially those

69 occurring during geomagnetic storms, are still one of the interesting issues to be fully

70 addressed. Some of the results showed that geomagnetic storms can affect the

71 development of EPBs (e.g., Abdu et al., 2003; Tulasi et al., 2008; Carter et al., 2016),

72 and in some extreme cases, the EPBs can extend to middle latitudes during intense

73 geomagnetic storms (e.g., Sahai et al., 2009; Patra et al., 2016; Katamzi-Joseph et al.,

74 2017; Aa et al., 2018). Moreover, in the storm time, EPBs near sunrise were

75 occasionally observed by some instruments such as radar and satellite. Fukao et al.

76 (2003) used observations from the Equatorial Atmosphere Radar to report EPBs near

77 sunrise over the Indonesian region during a geomagnetic storm and suggested that the

78 EPBs were likely associated with the geomagnetic storm. Huang et al. (2013) reported

79 the observations of long-lasting daytime EPBs with the Communications/Navigation

80 Outage Forecasting System (C/NOFS) satellite during a geomagnetic storm in which

81 the EPBs were persistent from the post-midnight sector through the afternoon sector.

82 Zhou et al. (2016) used observations from multiple low Earth orbiting satellites, like

83 the Swarm constellation, the Gravity Recovery and Climate Experiment (GRACE)

84 satellite, and the C/NOFS satellite, to detect the EPBs around sunrise during the St

3

Patrick's Day storm. They suggested that the geomagnetic storm induced changes in ionospheric dynamics should be the reason for triggering the EPBs. But until now, there has been no research on the occurrence characters and evolution of EPBs around sunrise using optical remote sensing, which can provide different aspects of the EPBs near sunrise.

It is well known that the EPBs usually drift eastward as reported by many studies (e.g., Pimenta et al., 2001; Martinis et al., 2003; Park et al., 2007; Taylor et al., 2013; Wu et al., 2017). However, during storm periods westward drifting EPBs have been also observed (Abdu et al., 2003; Basu et al., 2010; Santos et al., 2016). Abdu et al. (2003) reported some cases of EPBs that showed eastward drifts after sunset and later reversed to westward. Basu et al. (2010) reported that the westward drifting EPBs reached maximum velocities of about 80 - 120 m/s. Santos et al. (2016) also showed some EPBs of zonal drifts reversal (eastward to westward) during a geomagnetic storm, ~~in which~~and they suggested the reversal was caused by a vertical Hall electric field ~~caused~~ which induced by a zonal prompt penetration electric field (PPEF) in the ~~reversal.~~ presence of enhanced conductivity in the E region during night.

From six-year observations of airglow image located in the southern China, we found only one case of EPBs starting to appear near sunrise during the storm recovery phase on 08 November 2015. The EPBs appeared before sunrise, kept developing and vanished in about 1 hour after sunrise. Unlike the quiet-time eastward drifting EPBs, the EPBs drifted westward. In the rest, we provide a detailed analysis of this event. In section 2, we give a general description of the instruments. Observational results are showed in section 3. In section 4, we provide comparisons with previous studies as well as discussions. Finally, summary is given in section 5.

2. Instrumentation

2.1 All-sky imager

The airglow data used in this study are obtained from an all-sky imager, which is deployed at Qujing, China (Geographic: 25° N, 104° E; Geomagnetic: 15.1° N, 176°

4

114   E). Its location is indicated by the red star in Figure 1, and the blue circle represents the

115   projected regions with a radius of ~900 km (about 140° field of view (FOV))of the

116   all-sky imager at an altitude of 250 km. The all-sky imager consists of a CCD detector

117   (1024 × 1024 pixel), an interference filter (630.0 nm), and a fish-eye lens (FOV of 180°).

118   The integration time of the all-sky imager is 3 min.

119

120   **2.2   The Network of Global Navigation Satellite System (GNSS)**

121   The GNSS data used in this study are derived from the Crustal Movement Observation

122   Network of China (CMONOC), which consists of ~260 ground GNSS receivers

123   covering the mainland of China. The information of these GNSS receivers has been

124   given in previous publications (e.g., Aa et al., 2015; Yang et al., 2016; Zheng et al.,

125   2016). The residuals of total electron content (TEC) was processed using the similar

126   method as that described by Ding et al. (2014). Specifically, for each arc, the relative

127   phase TEC was filtered using a band-pass filter. The minimum and maximum period of

128   the band-pass filter was 2 min and 12 min respectively. We then calculated the TEC

129   residual of each arc for each pierce point, which the height of each ionospheric pierce

130   point was about 300 km. Therefore, the TEC residual could indicate the occurrence of

131   plasma bubbles. An elevation cutoff angle of 30° is used to reduce the multi-paths

132   effects. Besides, to better present the structure of EPBs, the rate of TEC change index

133   (ROTI) was also calculated. The ROTI is the standard deviation of the TEC gradient,

134   which is rate of TEC change (ROT). Based on (TEC(t+Δt)-TEC(t))/ Δt, we can get the

135   ROT. In the study, we used Δt =30s to calculate the ROT and used 10 ROT to get 5 min

136   ROTIs. Similar calculation of ROT and ROTI have already been reported and discussed

137   by many previous studies (e.g., Pi et al., Otsuka et al., 2006; Buhari et al., 2004), we

138   will not be described in here.

139

140   **2.3   Digisond**

141   **2.3   Digisonde**

142   The digisonde ionograms are obtained from a digisonde located at Fuke, a low-latitude

5

143 station in the southern China (Geographic: 19.5° N, 109.1° E; Geomagnetic: 9.5° N,

144 178.4° W), and marked with a green dot in Figure 1. The virtual heights of the *F* layer

145 were manually scaled by using the SAO Explorer software.

146

147 **3. Observations and Results**

148 Figure 2 shows the 3-hour *Kp* index, the interplanetary magnetic field (IMF) *Bz*, *SYM-*

149 *H*, AE, AU, AL and h' F at Fuke on 06-08 November 2015. To make the comparison

150 easier with other observations, we converted the universal time to the local time (LT)

151 at Qujing. A geomagnetic storm occurred during those days. In Figure 2(b), IMF *Bz*

152 turned southward at ~11:40 LT on 07 November 2015, and reached to about -11 nT at

153 ~16:00 LT. During the storm main phase, the *SYM-H* had a rapid reduction from -40 nT

154 to -100 nT. Meanwhile, the *Kp* index reached a value of 6; the AE and AL also reached

155 at ~1500 nT and ~- 1500 nT, respectively. After 04:00 LT on 08 November 2015, IMF

156 *Bz* began to turn to north. In the storm recovery phase, the value of *SYM-H* was back to

157 -40 nT.

158 Figure 3 shows the time sequence of airglow images observed by the all-sky imager at

159 Qujing from 05:15 to 06:21 LT on 8 November 2015. The time difference between

160 successive images is 6 min. For each image, we removed the effects of compression

161 and curving of the all-sky imager lens by an unwarping process (Garcia et al., 1997).

162 All images have been mapped into a geographic range from 97° to 111° E in longitude

163 and from 18° to 32° N in latitude. The height of the airglow layer is assumed to be at

164 250 km. The top of each image is to the north and the right to the east. Two EPBs,

165 marked as "b1" and "b2", were observed by the all-sky imager during this period. They

166 occurred during the geomagnetic storm recovery phase.

167 Around 05:21 LT, EPB "b1" appeared in the FOV of the all-sky imager. "b1" was still

168 developing, as it extended northward and reached close to 25° N around 06:21 LT. At

169 05:39 LT, the other EPB "b2" started to appear in the FOV of the airglow imager. "b2"

170 was also developing and expanded to about 20° N at 06:21 LT. The two observed EPBs

171 possibly continued to develop after 06:21 LT, as no hints of stop can be seen in the last

6

172 airglow image. However, there was no further image data after 06:21 LT because the

173 all-sky imager had to be shut down after sunrise. We want to pointed out that the sunrise

174 time at Qujing was around 06:15 LT at altitude of 250 km on that day. The far north

175 part of "b1" reached about 24.5°N at 06:15 LT. After 6 min, the far north of "b1"

176 extended to about 25°N (as marked by the black horizontal line). In other words, the

177 observational result from the all-sky imager suggested that the EPBs kept developing

178 after sunrise.

179 Some interesting features can also be seen from Figure 3. "b1" appeared at ~105° E and

180 "b2" appeared at ~104° E at 05:39 LT. Based on the black vertical line at 106° E, we

181 can clearly see that the two EPBs drifted from east to west. Besides, ~~break~~bifurcation

182 and ~~recombination~~merging processes of EPB "b1" were also observed. After 05:45 LT,

183 a ~~break~~bifurcation process occurred in "b1". The lower latitude portion of "b1" moved

184 further to the westward. An obvious cleft occurred at ~19° N of "b1" near 06:03 LT.

185 More interesting is the fact that a ~~recombination~~merging process occurred in the two

186 ~~break~~bifurcation portions of "b1" during its later development period. After ~06:03 LT,

187 the upper portion of "b1" began to connect to the lower portion of "b1" and they

188 merged/combined together into one EPB after 06:15 LT. The ~~break~~bifurcation and

189 ~~recombination~~merging processes are more obvious in the red rectangles of Figure 3,

190 which is indicated by the red arrow in each image.

191 Figure 4 shows a series of TEC residuals over 10°-50°N and 80°-130°E during 04:30-

192 08:20 LT on 08 November 2015. The adjacent imaging is in 10 min intervals. At about

193 04:40 LT, some TEC depletions, which occurred to the south and west of the location

194 of all-sky imager, appeared at ~115°E (~24°N), and began to develop. About 05:30 LT,

195 some additional EPBs appeared at ~105°E (~20°N), and they were also developing.

196 EPBs in the two regions kept developing until they disappeared. Owning to the FOV of

197 the all-sky imager, the EPBs outside the ~115°E region were not observed.

198 In order to provide much more detailed comparison between the all-sky imager and

199 TEC measurements, we ~~chose those~~give local time variation of the absolute TEC

200 ~~variations of~~after 05:15 LT (Figure 5) which corresponding geographical area ~~and time~~

7

201 of each airglow imaging of Figure 3 in Figure 5. In Figure 5, the TEC variations show

202 that the EPBsdepletions at ~105° E appeared near 05:30 LT, which correspond to EPB

203 "b1" and "b2" observed by the all-sky imager. In Figure 5,And after ~07:45 LT, those

204 TEC depletions disappeared. For a better representation, we showed ROTI variations

205 which correspond geographical area and time of each airglow imaging of Figure 3. In

206 Figure 6, the ROTI enhancement at ~105° E also correspond to EPB "b1" and "b2"

207 observed by the all-sky imager near 05:30 LT. The ROTI enhancement move away from

208 the 106° E with time (The black vertical line represents the 106°E in Figure 56), which

209 is consistent with the movement of EPBs observed by the airglow imager. Meanwhile,

210 the northernmost part of the depletion of ~105°EROTI enhancement expanded to

211 ~25°N at 06:2021 LT (The black horizontal line represents the 25°N in Figure 56),

212 which also agreed well with the observations of the all-sky imager. Interestingly, In

213 Figure 4, TEC variationsresiduals show that the northernmost of EPBs of ~105°E

214 extended beyond 25°N after 06:20 LT. We can see that the northernmost of them

215 reached about 28°N at 07:10 LT in Figure 4. In other words, TEC variations show that

216 thethose depletions of ~105°E were still thereexistence after 06:21 LT, and kept

217 developing after sunrise, but vanished afternear ~08:00 LT. These observational results

218 shown that the life time of those EPBs exceeds 3 hours.

219

220 **4. Discussion**

221 In this study we showed an special event of EPBs which was simultaneously observed

222 by the all-sky imager and the ground GNSS network in the south China. One interesting

223 feature is that the EPBs started to appear near sunrise hours. Afterward, they kept

224 developing until they totally vanished. During their life time, the EPBs moved from

225 east to west. Those EPBs occurred in the recovery phase of the geomagnetic storm,

226 which indicates that the prompt penetration electric fields (PPEF) and disturbance

227 dynamo (DDEF), as well as disturbed neutral wind circulation may play an import role

228 in triggering the EPBs.

229 The drift velocities of EPBs were shown in Figure 67. We used the cross sections

230 (keogram) (Figures 67 (a), (c), and (e)) of the airglow images to separately calculate

8

231 meridian velocities (Figure 67(b)) of "b1" and zonal velocities of "b1" at ~ 22°N

232 (Figure 67(d)) and ~19°N (Figure 67(f)) geographical latitudes. Figure 67(a) illustrates

233 the N-S cross sections (between 104°E and 105°E) of the airglow images shown in

234 Figure 3. Figure 67(c) illustrates the W-E cross sections (between 21.5°N and 22°N) of

235 the airglow images, and Figure 67(e) illustrates the W-E cross sections (between 18.5°N

236 and 19°N).

237 We separately calculated poleward and zonal velocities of "b1" based on the position

238 of it changed over time in Figure 67(a), Figure 67(c) and Figure 67(e). The initial

239 poleward and zonal velocities of "b1" were about 200 m/s and 60 m/s, respectively.

240 Horizontal drift of EPB is also an important issue, which is often related to the

241 background zonal plasma drift (Fejer et al., 2005; Eccles, 1998). The westward motion

242 of the F-region should be caused by the ionospheric dynamo process in the early

243 morning (Kil et al., 2000; Sheehan &and Valladares, 2004). The drift direction of

244 background zonal plasma drift has a reversal (eastward to westward) near dawn (Fejer

245 et al., 2005). Huang and Roddy. (2015) also found the drift velocity of EPBs was

246 eastward at night and reverses to westward near dawn by using data from C/NOFs and

247 they showed enhanced geomagnetic activities caused a westward EPB drift in the

248 nighttime through disturbance dynamo process. In our case, all EPBs emerged after

249 05:00 LT. The background plasma should drift westward during the early morning hours.

250 So, it could partly explain why the observed EPBs drifted westward. In addition, the

251 disturbed westward neutral winds can also contribute to the westward drifting of EPBs.

252 Xiong et al. (2015) found that the disturbance winds were mainly towards westward at

253 low latitudes, most prominent during early morning hours. Abdu et al. (2003) found

254 that the westward drift of an EPB was most likely caused by westward zonal winds

255 during a geomagnetic storm. Makela et al. (2006) found that the eastern wall of EPBs

256 can become unstable due to the westward and equatorward neutral winds associate with

257 wind surges. When the wind blow westward, and thus the wind-induced Pedersen

258 current flows downward, gradient-drift instability can occur at the eastern wall of EPB,

259 where the plasma density gradient is eastward. So, secondary instabilities are more

9

260 likely to occur at eastern wall of EPBs. In Figure 3, a sub-branch of dark bands first

261 occurred at the eastern wall of "b1", indicated secondary instabilities developed at the

262 eastern edge, most likely due to the westward disturbance winds.

263 In Figure 78, we used the Thermosphere-Ionosphere-Electrodynamics General

264 Circulation Model (TIE-GCM) to simulate the horizontal winds on 08 November 2015

265 under magnetically active conditions, and the latitude versus longitude distribution of

266 zonal wind velocities are shown at different times. The winds at 250 km are shown, and

267 the spatial coverage has been confined to 0° - 40° N latitude and 90° - 120° E longitude.

268 The dashed rectangles represent the location of "b1" and "b2" at different times. In

269 Figure 78, we can see that the horizontal winds at low latitudes are mainly westward,

270 which is consistent with the motion of EPBs in this case. As already discussed above,

271 the westward drift of those EPBs is possibly caused by the westward disturbance winds.

272 Besides, the zonal winds computed from TIE-GCM shown in Figure 78 are smaller

273 than the zonal drifts of EPBs shown in Figure 67. This is because zonal drift value of

274 EPBs was controlled by background zonal winds and ionospheric electric field

275 (Haerendel et al., 1992; Eccles, 1998). The value differences between simulation and

276 zonal drifts of EPBs should be influenced by ionospheric electric field. Besides, The

277 difference between the model simulated background zonal winds and the derived zonal

278 drifts of EPBs from airglow images is possibly due to that the model simulation provide

279 mainly reflect a general trend of the wind, but not the exact wind velocity in reality.

280 As reported, most of the EPBs start to occur at pre-midnight hours. There were a very

281 limited number of studies that used data from radar or satellite to report the occurrence

282 of EPB close to sunrise hours (e.g., Fukao et al., 2003; Huang et al., 2013; Zhou et al.,

283 2016). However, until now, there has been no observation result of EPBs around sunrise

284 using optical remote sensing. In fact, it is very difficult to observe EPB near sunrise by

285 an all-sky imager. Often, EPBs start to develop shortly after sunset and vanish before

286 sunrise. Even though some EPBs occur around sunrise in their initial stage, they

287 disappear when they drift eastward into the daytime. And almost no report shows that

288 the EPBs still kept developing after sunrise. In our case, the developing EPB was first

10

289 observed at about 05:30 LT (near dawn) by both the all-sky imager and the GNSS

290 network. The local time variation of absolute TEC showed that EPBs existed after

291 sunrise and they disappeared after 07:45 LT. Our observational results show that they

292 kept developing after sunrise, and vanished about one hour after sunrise. Those EPBs

293 should be occurred near sunrise, which is different from post-sunset EPBs. Their

294 development stages lasted for at least about 3 hours.

295 In the rest, we try to explain why the EPBs occurred near sunrise. During the storm

296 time, disturbance winds can affect the low-latitude ionospheric electrodynamics as well

297 as the zonal drift of an EPB. The DDEF caused by storm will drive plasma drift to move

298 upward atduring nighttime during the development phase of storm (Blanc and

299 Richmond, 1980). Meanwhile, a number of studies found the that high latitude electric

300 fields can penetrate into the middle and low-latitude ionosphere as PPEF when IMF Bz

301 turns southward or northward (Kelley et al., 1979; Scherliess and Fejer, 1997; Cherniak

302 &and Zakharenkova, 2016; Carter et al., 2016; Patra et al., 2016; Katamzi-Joseph et al,

303 2017). For the storm event, after IMF Bz turned southward at ~12:00 LT 07 November

304 2015, there was long duration and high AE in storm time. A DDEF should be present

305 at recovery phase of storm time. And it reversed ambient electric field from westward

306 to eastward near sunrise, which enhanced height of bottomside of the ionosphere F-

307 region. Meanwhile, the northward turning of IMF Bz at ~04:00 LT 08 November 2015

308 caused over- shielding electric field, which produced an eastward PPEF into the low-

309 middle latitude ionosphere. The eastward electric field also moved the F region

310 ionosphere to higher altitudes via vertical $E \times B$ drifts. In Figure 2(e), the increased

311 height of bottomside of the ionosphere F-region can be seen at Fuke. In low latitude

312 region, one of the necessary conditions for the generation of EPBs is that the F layer

313 should be uplifted to a higher altitude, where the RTI becomes unstable and forms EPBs.

314 The F layer height is largely determined by the eastward field via the vertical $E \times B$ drift

315 (Dabas et al., 2003).

316 In this study, EPBs were initially observed by the all-sky imager at about 05:15 LT. We

317 think that only a portion of the EPBs were observed in our study, as EPB usually extend

11

318   along the whole magnetic flux-tube. It also means that the EPBs should possibly occur

319   before 05:15 LT at equatorial latitude. But due to the lack of observations at equator,

320   we cannot provide direct evidence about their generation. However, as shown in our

321   Figure 89, we also found that spread F began to appear in the ionograms from the

322   digisonde at Fuke after 05:15 LT, which indicates that those EPBs occurred in the region

323   of southeastern Qujing (Note that Fuke is to the southeast of Qujing). Bottomside of

324   the ionospheric F-region at Fuke was rapidly elevated from ~250 km to ~290 km near

325   sunrise on 08 November 2015. The rapidly elevated height of the ionosphere can cause

326   stronger RTI at the bottom of the ionosphere F-region, which is beneficial to the

327   formation of EPB. The initial occurring time of EPBs of this case should be during this

328   time. Unfortunately, we do not have more observations in the southeast of Fuke. We

329   used the TIE-GCM to simulate the height of hmF2 at lower latitude on 08 November

330   2015. Figure 910 shows the hmF2 as a function of longitude and latitude at different

331   times. The model results plotted are in a geographic range from 0° to 40° N in latitude

332   and from 90° to 120° E in longitude. In Figure 910, we can see that hmF2 southeast of

333   (the dashed rectangles) Qujing was rapidly elevated to higher altitudes near sunrise. In

334   other words, when the IMF Bz turned northward at about 04:00 LT, the ionosphere in

335   some regions southeast of Qujing could be rapidly elevated to higher altitudes at this

336   time. Those EPBs occurred in the same time period as highlighted by the green

337   rectangular area in Figure 2. Previous studies have reported that the occurrence of the

338   dawn enhancement in the equatorial ionospheric vertical plasma drift (Zhang et al.,

339   2015, 2016). They found that the enhancement of the ionospheric vertical plasma drift

340   occurs around dawn. They suggested that the vertical plasma drifts can be enhanced

341   near sunrise in a way similar to the PRE near sunset. Fejer et al. (2008) found that the

342   nighttime disturbance dynamo drifts are upward, and have the largest values near

343   risesunrise. In our case, the model simulations and observations both show an

344   increasing of the height of the ionosphere around sunrise. The enhancement of low-

345   latitude ionospheric vertical plasma drift caused by DDEF and PPEF associated with

346   the geomagnetic storm should play a vital role in triggering those EPBs. Our results

12

347 also provide evidence of the enhancement of low-latitude ionospheric vertical plasma

348 drift around sunrise, which should be the main reason of the EPBs generation near dawn.

349 In addition, some interesting features of EPBs are also shown in Figure 3 in that the

350 EPBs showed also bifurcation and merging processes. Merging phenomenon of EPBs

351 has been studied by some researchers (Huang et al., 2012; Huba et al., 2015; Narayanan

352 et al., 2016; Wu et al., 2017). break and recombination processes. In Figure 6 However,

353 there is no study to report that bifurcation first and merging later occur in evolution of

354 one EPBs. In Figure 7(f), at latitude of 19°N, the zonal velocity of "b1" was about 60-

355 70 m/s between 05:20 LT and 06:15 LT. However, at the latitude of 22°N (Figure 67(d)),

356 the zonal velocity of "b1" was decreased from about 70 m/s to about 50 m/s between

357 05:20 LT and 05:45 LT. After 05:45 LT, its velocity began to increase from ~50 m/s to

358 ~70 m/s from 05:45 LT to 06:00 LT. Then, it kept a velocity of ~70 m/s. Owning to the

359 fact that the zonal velocity at higher latitudes was smaller than that at low latitudes

360 before 05:45 LT, "b1" had a breakbifurcation process of EPBs during this period. After

361 05:45 LT, the zonal velocity at higher latitude was bigger than that at lower latitude,

362 "b1" exhibited a recombinationmerging process of EPBs after 06:03 LT. The above

363 results indicate that the breakbifurcation and recombinationmerging processes of EPBs

364 should be caused by the different drift velocities of the background plasma at different

365 latitudes.

366

367 **5. Summary**

368 In this paper, a special EPB event was observed by an all-sky imager and the GNSS

369 network in the southern China. The evolution processes and characteristics of those

370 EPBs were studied in detail. Our main findings are summarized as below:

371 (1) The observed EPBs on 08 November 2015 emerged before sunrise and kept

372   developing. They dissipated at about one hour after sunrise (~ after 08:00 LT) and

373   the development stage lasted for at least about 3 hours. The evolution of EPBs

374   developing around sunrise was observed for the first time by an all-sky imager and

375   the GNSS network.

376 (2) They occurred in the recovery phase of a geomagnetic storm. The enhancement of

13

377   background ionospheric vertical plasma drift was also observed near sunrise. The

378   rapid uplift of the ionospheric caused by the geomagnetic storm should be the main

379   reason for triggering the EPBs.

380   (3) During the development, the EPBs drifted westward rather than eastward, The TIE-

381   GCM simulation suggested that the westward drift of EPB is related to the westward

382   disturbance winds.

383   (4) The EPB exhibited also ~~break~~bifurcation and ~~recombination~~merging processes

384   during its development.

14

15

References

Aa, E., Huang, W., Yu, S., Liu, S., Shi, L., & Gong, J., et al. (2015)., Chen, Y and Shen, H.: A regional ionospheric tec mapping technique over china and adjacent areas on the basis of data assimilation. *Journal of Geophysical Research: Space Physics,* J. Geophys. Res., 120(6), 5049-5061. https://doi.org/10.1002/2015JA021140, 2015.

Aa, E., Huang, W., Liu, S., Ridley, A., Zou, S., Shi, L., et al. (2018).Chen, Y., Shen, H., Yuan, T., Li, J., and Wang, T.: Midlatitude plasma bubbles over China and adjacent areas during a magnetic storm on 8 September 2017. Space Weather, 16, 321–331. https://doi.org/10.1002/2017SW001776, 2018.

Abdu, M. A. (2001).: Outstanding problems in the equatorial ionosphere–thermosphere electrodynamics relevant to spread f. *Journal of Atmospheric and Solar-Terrestrial Physics,* J. Atmos. Sol. Terr. Phys., 63(9), 869-884. https://doi.org/10.1016/S1364-6826(00)00201-7, 2001.

Abdu, M. A. (2003).: Magnetospheric disturbance induced equatorial plasma bubble development and dynamics: A case study in Brazilian sector. *Journal of Geophysical Research,* J. Geophys. Res., 108(, A12). https://doi.org/10.1029/2002ja009721, 2003.

Basu, S., Basu, S., MacKenzie, E., Bridgwood, C., Valladares, C. E., Groves, K. M., &and Carrano, C. (2010).: Specification of the occurrence of equatorial ionospheric scintillations during the main phase of large magnetic storms within solar cycle. Radio Science, 45, RS5009. https://doi.org/10.1029/2009RS004343, 2010.

Blanc, M. &, and Richmond, A. D. (1980).: The ionospheric disturbance dynamo. *Journal of Geophysical Research: Space Physics,* J. Geophys. Res., 85(, A4). https://doi.org/10.1029/JA085iA04p01669. 1980.

Buhari, S. M. , Abdullah, M. , Hasbi, A. M. , Otsuka, Y. , Yokoyama, T. , & Nishioka, M.: Continuous generation and two‐dimensional structure of equatorial plasma bubbles observed by high‐density gps receivers in southeast asia, J. Geophys.

16

Res.,119, 12, https://doi.org/10.1002/2014JA020433, 2014.

Burke, W. J., Gentile, L. C., Huang, C. Y., Valladares, C. E., &and Su, S. Y. (2004).: Longitudinal variability of equatorial plasma bubbles observed by dmsp and rocsat-1. *Journal of Geophysical Research,* , J. Geophys. Res., 109(A12), 17., https://doi.org/10.1029/2004JA010583, 2004.

Carter, B. A., Yizengaw, E., Pradipta, R., Retterer, J. M., Groves, K., & Valladares, C., et al. (2016).Caton, R., Bridgwood, C., Norman, R., and Zhang, K.: Global equatorial plasma bubble occurrence during the 2015 St. Patrick's day storm. *Journal of Geophysical Research Space Physics,* , J. Geophys. Res., 121(1), 894-905., https://doi.org/10.1002/2015JA022194, 2016.

Cherniak, I., &and Zakharenkova, I. (2016). : First observations of super plasma bubbles in Europe. *Geophysical Research Letters,* , Geophys. Res. Lett., 43, 11,137–11,145., https://doi.org/10.1002/2016GL071421, 2016.

Dabas, R. S. ,, Singh, L. ,, Lakshmi, D. R. ,, Subramanyam, P. , Chopra, P. , &and Garg, S. C. . (2003). : Evolution and dynamics of equatorial plasma bubbles: relationships to exb drift, postsunset total electron content enhancements, and equatorial electrojet strength. Radio Science, . 38(4), 1075., https://doi.org/10.1029/2001RS002586, 2003.

Ding, F., Wan, W., Mao, T., Wang, M., Ning, B., Zhao, B., &and Xiong, B. (2014). : Ionospheric response to the shock and acoustic waves excited by the launch of the Shenzhou 10 spacecraft. *Geophysical Research Letters,* , Geophys. Res. Lett., 41, 3351–3358., https://doi.org/10.1002/2014GL060107, 2004.

Eccles., Vincent,V. J. (1998). : A simple model of low-latitude electric fields. *Journal of Geophysical Research,* , J. Geophys. Res., 103(A11), 26699-26708., https://doi.org/10.1029/98JA02657, 1998.

Fukao, S., Ozawa, Y., Yamamoto, M., and Tsunoda, R. T. (2003). : Altitude extended equatorial spread F observed near sunrise terminator over Indonesia. Geophys. Res. Lett., 30(22), 2137. https://doi.org/10.1029/2003GL018383, 2003.

Fejer, B. G., &and Scherliess, L. (1998). : Mid- and low-latitude prompt-penetration

17

ionospheric zonal plasma drifts. *Geophysical Research Letters,*, Geophys. Res. Lett., 25(16),, 3071–3074. https://doi.org/10.1029/98GL02325, 1998.

Fejer, B. G., Scherliess, L., &and Paula, E. R. D. (1999).: Effects of the vertical plasma drift velocity on the generation and evolution of equatorial spread-f. *Journal of Geophysical Research Space Physics,*, J. Geophys. Res., 104, 19,-859-19,-869-. https://doi.org/10.1029/1999JA900271, 1999.

Fejer, B. G., Souza, J. R., Santos, A. S., &and Pereira, A. E. C. (2005).: Climatology of F, region zonal plasma drifts over Jicamarca. *Journal of Geophysical Research,* , J. Geophys. Res., 110, A12310-. https://doi.org/10.1029/2005JA011324, 2005.

Fejer, B. G., Jensen, J. W., &and Su, S.-Y. (2008).: Seasonal and longitudinal dependence of equatorial disturbance vertical plasma drifts. Geophysical Research Letters,, Geophys. Res. Lett., 35(, 20).. https://doi.org/10.1029/2008gl035584, 2008.

Garcia, F. J., Taylor, M. J., &and Kelley, M. C. (1997).: Two-dimensional spectral analysis of mesospheric airglow image data-. Applied Optics,-., 36(29),, 7374-. https://doi.org/10.13 64/AO.36.007374, 1997.

Haerendel, G., Eccles, J. V., &and Çakir, S. (1992).: Theory for modeling the equatorial evening ionosphere and the origin of the shear in the horizontal plasma flow. *Journal of Geophysical Research,*, J. Geophys. Res., 97(A2),, 1209–1223-. https://doi.org/10.1029/91JA02226, 1992.

Huang, C.-S., J. M. Retterer, O. de La Beaujardiere, P. A. Roddy, D. E. Hunton, J. O. Ballentin, and R. F. Pfaff.: Observations and simulations of formation of broad plasma depletions through merging process, J. Geophys. Res., 117, A02314, https://doi:10.1029/2011JA017084.-l, 2012.

Huang, C. S. , Beaujardiere, O. D. L. , Roddy, P. A. , Hunton, D. E. , Ballenthin, J. O. , &and Hairston, M. R. (2013).: Long-lasting daytime equatorial plasma bubbles observed by the c/nofs satellite. *Journal of Geophysical Research Space*

18

Physics, J. Geophys. Res., 118(5), 2398-2408. https://doi.org/10.1002/jgra.50252, 2013.

Huang, C. S. (2018).Huang, C. S. , and Roddy, P. A.: Effects of solar and geomagnetic activities on the zonal drift of equatorial plasma bubbles, J. Geophys. Res., 121, 628-637, https://doi.org/10.1002/2015JA021900, 2016.

Huang, C. S.: Effects of the postsunset vertical plasma drift on the generation of equatorial spread f., Progress in Earth &and Planetary Science., 5(1), 3. https://doi.org/10.1186/s40645-017-0155-4, 2018.

Huba, J. D., T.-W. Wu, and J. J. Makela.: Electrostatic reconnection in the ionosphere, Geophys. Res. Lett., 42, 1626–1631, https://doi:10.1002/2015GL063187, 2015.

Katamzi-Joseph, Z. T., Habarulema, J. B., &and Hernández-Pajares, M. (.2017). Midlatitude postsunset plasma bubbles observed over Europe during intense storms in April 2000 and 2001., Space Weather., 15, 1177–1190. https://doi.org/10.1002/2017SW001674, 2017.

Kelley, M. C., Fejer, B. G., &and Gonzales, C. A. (1979).: An explanation for anomalous equatorial ionospheric electric fields associated with a northward turning of the interplanetary magneticfield. *Geophysical Research Letters,*, Geophys. Res. Lett., 6, 301-304. https://doi.org/10.1029/GL006i004p00301, 1979.

Kelley, M. C., et al. (1986).Labelle, J., Kudeki, E., Fejer, B. G., Basu, S., Baker, K. D., Hanuise, C., Argo, P., Woodman, R.F., Swartz, W. E., Farley, D., and Meriwether, J.: The Condor Equatorial Spread F Campaign: Overview and results of the large-scale measurements. *Journal of Geophysical Research,*, J. Geophys. Res., 91(A5), 5487–5503. https://doi.org/10.1029/JA091iA05p05487,1986.

Kelley, M. C. (2009).: The Earth's Ionosphere: Plasma Physics and Electrodynamics. San Diego, CA: Academic, 2009.

Kil, H., Kintner, P. M., De Paula, E. R., &and Kantor, I. J. (2000).: Global positioning system measurements of the ionospheric zonal apparent velocity at cachoeira paulista in brazil. *Journal of Geophysical Research Space Physics,*, J. Geophys.

19

Res., 105(A3), 5317-5327. https://doi.org/10.1029/1999JA000244, 2000.

Lühr H., Xiong, C., Park, J., and Rauberg, J. (2014).: Systematic study of intermediatescale intermediate scale structures of equatorial plasma irregularities in the ionosphere based on CHAMP observations. Front Phys., 2, 15. https://doi.org/10.3389/fphy.2014.00015, 2014.

Makela, J. J., Kelley, M. C., &, and Nicolls, M. J. (2006).: Optical observations of the development of secondary instabilities on the eastern wall of an equatorial plasma bubble. Journal of Geophysical Research Space Physics, J. Geophys. Res., 111(A9), . https://doi.org/ 10.1029/2006JA011646, 2006.

Makela, J. J., and Otsuka, Y. (2012).: Overview of Nighttime Ionospheric Instabilities at Low-and Mid-Latitudes: Coupling Aspects Resulting in Structuring at the Mesoscale. Space Science Reviews, 168, 419. https://doi.org/10.1007/s11214-011-9816-6, 2012.

Martinis, C., Eccles, J. V., Baumgardner, J., Manzano, J., & and Mendillo, M. (2003).: Latitude dependence of zonal plasma drifts obtained from dual‐site airglow observations. Journal of Geophysical Research Space Physics, J. Geophys. Res., 108(A3). https://doi.org/10.1029/2002JA009462, 2003.

Narayanan, V. L., S. Gurubaran, and K. Shiokawa.: Direct observational evidence for the merging of equatorial plasma bubbles, J. Geophys. Res. Space Physics,121, 7923–7931, https://doi:10.1002/2016JA022861, 2016.

Ott, E. (1978).: Theory of Rayleigh-Taylor bubbles in the equatorial ionosphere. Journal of Geophysical Research, J. Geophys. Res., 83(A5), 2066. https://doi.org/10.1029/JA083ia05p02066, 1978.

Otsuka, Y., T. Aramaki, T. Ogawa, and A. Saito.: A statistical study of ionospheric irregularities observed with a GPS network in Japan, in Recurrent Magnetic Storms: Corotating Solar Wind Streams, Geophys. Monogr. Ser., vol. 167, edited by B. T. Tsurutani et al., AGU, Washington, D. C, 2006.

Park, S. H., England, S. L., Immel, T. J., Frey, H. U., & and Mende, S. B. (2007).: A method for determining the drift velocity of plasma depletions in the equatorial

20

ionosphere using far‐ultraviolet spacecraft observations. *Journal of Geophysical Research Space Physics*, J. Geophys. Res., 112(, A11). https://doi.org/10.1029/2007/JA012327, 2007.

Pi, X., A. J. Mannucci, U. J. Lindqwister, and C. M. Ho.: Monitoring of global ionospheric irregularities using the worldwide GPS network, Geophys. Res. Lett., 24,18, 2283–2286, https://doi.org/10.1029/97GL02273, 1997.

Pimenta, A. A., Fagundes, P. R., Bittencourt, J. A., Sahai, Y., Gobbi, D., &-Medeiros, A. F., et al. (2001).Taylor, M. J., and Takahashi, H.: Ionospheric plasma bubble zonal drift: a methodology using oi 630 nm all-sky imaging systems‐. Advances in Space Research,. 27(6), 1219-1224. https://doi.org/10.1016/s0273-1177(01)00201-0, 2001.

Patra, A. K., Chaitanya, P. P., Dashora, N., Sivakandan, M., &and Taori, A. (2016). : Highly localized unique electrodynamics and plasma irregularities linked with the 17 march 2015 severe magnetic storm observed using multitechnique common‐volume observations from gadanki, india. *Journal of Geophysical Research Space Physics*, J. Geophys. Res., 121.11,518-11,527. https://doi.org/10.1002/2016JA023384, 2016.

Sahai, Y., Becker-Guedes, F., Fagundes, P. R., de Jesus, R., de Abreu, A. J., Otsuka, Y., et al. (2009).Shiokawa, k., Igarashi, K., Yumoto, K., Huang, C. S., Lan, H. T., Saito, A., Guarnieri, F. L., Pillat, V. G., and Bittencourt, J. A.: Effects observed in the ionospheric F region in the east Asian sector during the intense geomagnetic disturbances in the early part of November 2004. *Journal of Geophysical Research*, J. Geophys. Res., 114, A00A18. https://doi.org/10.1029/2008JA013053. 2009.

Santos, A. M., Abdu, M. A., Souza, J. R., Sobral, J. H. A., Batista, I. S., &and Denardini, C. M. (2016). : Storm time equatorial plasma bubble zonal drift reversal due to disturbance Hall electric field over the Brazilian region. *Journal of Geophysical Research: Space Physics*, J. Geophys. Res., 121, 5594–5612. https://doi.org/10.1002/2015JA022179, 2016.

21

575 Sheehan, R. E., ~~&~~and Valladares, C. E~~. (2004).~~.: Equatorial ionospheric zonal drift

576 model and vertical drift statistics from UHF scintillation measurements in South

577 America~~. Annales Geophysicae~~, Ann. Geophys., 22~~(9)~~, 3177–3193~~.~~,

578 https://doi.org/10.5194/angeo-22-3177-2004, 2004.

579 Scherliess, L., ~~&~~and Fejer, B. G~~. (1997).~~.: Storm time dependence of equatorial

580 disturbance dynamo zonal electric fields~~. Journal of Geophysical Research: Space~~

581 ~~Physics~~, J. Geophys. Res., 102~~(A11)~~, 24037–24046~~.~~,

582 https://doi.org/10.1029/97ja02165, 1997.

583 Taylor, M. J., Eccles, J. V., Labelle, J., ~~&~~and Sobral, J. H. A~~. (2013).~~.: High resolution

584 oi (630 nm) image measurements of f‑region depletion drifts during the guará

585 campaign~~. Geophysical Research Letters~~, Geophys. Res. Lett., 24~~(13)~~, 1699-

586 1702~~.~~, https://doi.org/10.1029/97gl01207, 2013.

587 Tulasi, R. S., Rama, R. P. V. S., Prasad, D. S. V. V. D., Niranjan, K., Gopi, K. S., ~~&~~and

588 Sridharan, R~~., et al. (2008).~~.: Local time dependent response of postsunset esf

589 during geomagnetic storms~~. Journal of Geophysical Research Space Physics~~, J.

590 Geophys. Res., 113, A07310~~.~~, https://doi.org/10.1029/2007/JA012922, 2008.

591 Weber, E., Buchau, J., ~~&~~and Moore, J~~. (1980).~~.: Airborne studies of equatorial F layer

592 ionospheric irregularities~~. Journal of Geophysical Research~~, J. Geophys.

593 Res., 85~~(A9)~~, 4631–4641~~.~~, https://doi.org/10.1029/JA0 85iA09p04631, 1980.

594 Xiong, C., Park, J., Lühr, H., Stolle, C., ~~&~~and Ma, S.Y~~. (2010).~~.: Comparing plasma

595 bubble occurrence rates at CHAMP and GRACE altitudes during high and low

596 solar activity~~. Annales Geophysicae~~, Ann. Geophys., 28, 1647-1658~~.~~,

597 https://doi.org/10.5194/angeo-28-1647-2010, 2010.

598 Xiong, C., Lühr, H., ~~&~~and Fejer, B. G~~. (2015).~~.: Global features of the disturbance

599 winds during storm time deduced from CHAMP observations~~. Journal of~~

600 ~~Geophysical Research: Space Physics~~, J. Geophys. Res., 120, 5137–5150~~.~~,

601 https://doi.org/10.1002/2015JA021302, 2015.

602 Xiong, C., Stolle, C., Lühr, H., Park, J., Fejer, B. G., and Kervalishvili, G. N~~. (2016)~~,.:

603 Scale analysis of the equatorial plasma irregularities derived from Swarm

22

constellation, Earth Planets Space, 68, 121, https://doi.org/10.1186/s40623-016-0502-5, 2016.

Xiong, C., Xu, J., Wu, K., and Yuan, W.: Longitudinal thin structure of equatorial plasma depletions coincidently observed by swarm constellation and all-sky imager, J. Geophys. Res., 123(3), https://doi.org/10.1002/2017JA025091, 2018.

Wu, K., Xu, J., Wang, W., Sun, L., Liu, X., and Yuan, W.: Interesting equatorial plasma bubbles observed by all-sky imagers in the equatorial region of China, J. Geophys. Res., 122, https://doi.org/10.1002/2017JA024561, 2017.

Wu, K., Xu, J., Xiong, C., and Yuan, W.: Edge plasma enhancements of equatorial plasma depletions observed by all-sky imager and the C/NOFS satellite, J. Geophys. Res., 123, 8835-8849, https://doi.org/10.1029/2018JA025809, 2018.

Yang, Z., Song, S., Jiao, W., Chen, G., and Xue, J.: Ionospheric tomography based on gnss observations of the cmonoc: performance in the topside ionosphere, GPS Solutions, 21(2), 363-375, https://doi.org/10.1007/s10291-016-0526-0, 2016.

Zhang, R., Liu, L., Chen, Y., and Le, H.: The dawn enhancement of the equatorial ionospheric vertical plasma drift, J. Geophys. Res., 120, 10,688-10,697, https://doi.org/10.1002/2015JA021972, 2015.

Zhang, R., Liu, L., Le, H., and Chen, Y.: Evidence and effects of the sunrise enhancement of the equatorial vertical plasma drift in the F region ionosphere, J. Geophys. Res., 121, 4826-4834, https://doi.org/10.1002/2016JA022491, 2016.

Zheng, J. , Zhao, B. , Xiong, B. , and Wan, W.: Spatial and temporal analysis of the total electron content over china during 2011–2014, Advances in Space Research, 57(12), https://doi.org/10.1016/j.asr.2016.03.037, 2016.

23

633   Zhou, Y. L~~.,~~, Lühr, Hermann, Xiong, C~~., &~~, and Pfaff, R. F~~. (2016)~~.: Ionospheric

634   storm effects and equatorial plasma irregularities during the 17-18 march 2015

635   event~~. *Journal of Geophysical Research: Space Physics.*~~, J. Geophys. Res., 121,

636   9146-9163, https://doi.org/10.1002/2016JA023122, 2016.

24

637 **Figure Captions**

638 **Figure 1.** The location of observation instruments. The red star denotes the geographic

639 location of the all-sky imager at Qujing (25° N, 104° E). The blue circle denotes the

640 field of view of the all-sky imager at an altitude of 250 km. The green dot denotes the

641 geographic location of the digisond at Fuke (19.5° N, 109.1° E). The red dotted line

642 represents the magnetic equator.

643

644 **Figure 2.** (a) *Kp* indexes, (b) the interplanetary magnetic field (IMF) *Bz*, (c) SYM/H,

645 and (d) AE, AU, AL during 06-08 November 2015. (e) The variations of h'F obtained

646 from the digisond at Fuke on 06-08 November 2015.

647

648 **Figure 3.** Images of equatorial plasma bubbles from the Qujing site between 05:15 LT

649 and 06:21 LT on 08 November 2015. The observed images were mapped into

650 geographical coordinates by assuming that the airglow emission layer was at an altitude

651 of ~250 km. The white vertical line is a reference line of 106° E and horizontal line is

652 a reference line of 25° N.

653

654 **Figure 4.** Total electron content residuals over China and adjacent areas with 10 minute

655 interval during 04:30 – 08:20 LT on 08 November 2015. The black horizontal line is a

656 reference line of 25° N.

657

658 **Figure 5.** ~~Total electron content residuals~~Two-dimensional map of absolute TEC during

659 05:15 – 08:00 LT on 08 November 2015.

660

661 **Figure 6.** Two-dimensional map of rate of TEC index (ROTI) correspond to each image

662 of Figure 3. The black horizontal line is a reference line of 25° N. The black vertical

663 line is a reference line of 106° E.

664

665 **Figure ~~6~~7.** (a) N-S cross sections (between 104°E and 105°E) of the airglow images on

25

666 08 November 2015. (c) W-E cross sections (between 21.5°N and 22°N) of the airglow

667 images. (e) W-E cross sections (between 18.5°N and 19°N) of the airglow images. (b)

668 The variations of the meridian velocities of "b1" with local time. (d) and (f) The

669 variations of the zonal velocities of "b1" at ~ 22°N and ~19°N geographical latitudes,

670 respectively.

671

672 **Figure 78.** Contours of nighttime zonal winds at 250 km in a range from 0° to 40° N in

673 latitude and from 90° to 120° E in longitude during 08 November 2015. The dashed

674 rectangles represent the location of EPBs.

675

676 **Figure 89.** The ionograms observed by the digisonde at Fuke between 04:00 LT and

677 07:30 LT on 08 November 2015.

678

679 **Figure 910.** The height of hmF2 in a range from 0° to 40° N in latitude and from 90°

680 to 120° E in longitude during 08 November 2015. The red star represent the location of

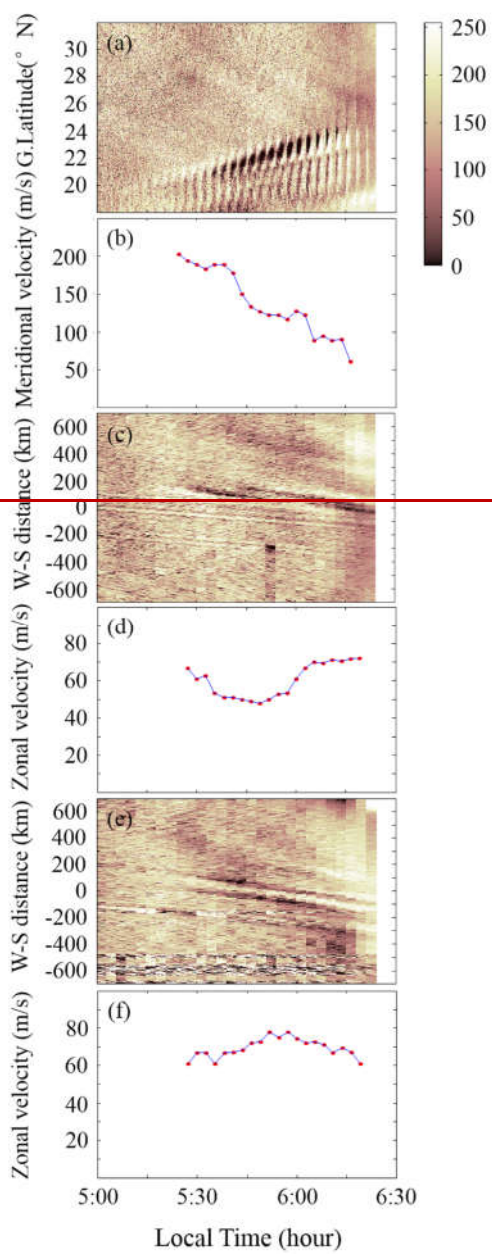681 all-sky imager. The dashed rectangles represent the region of southeastern Qujing.
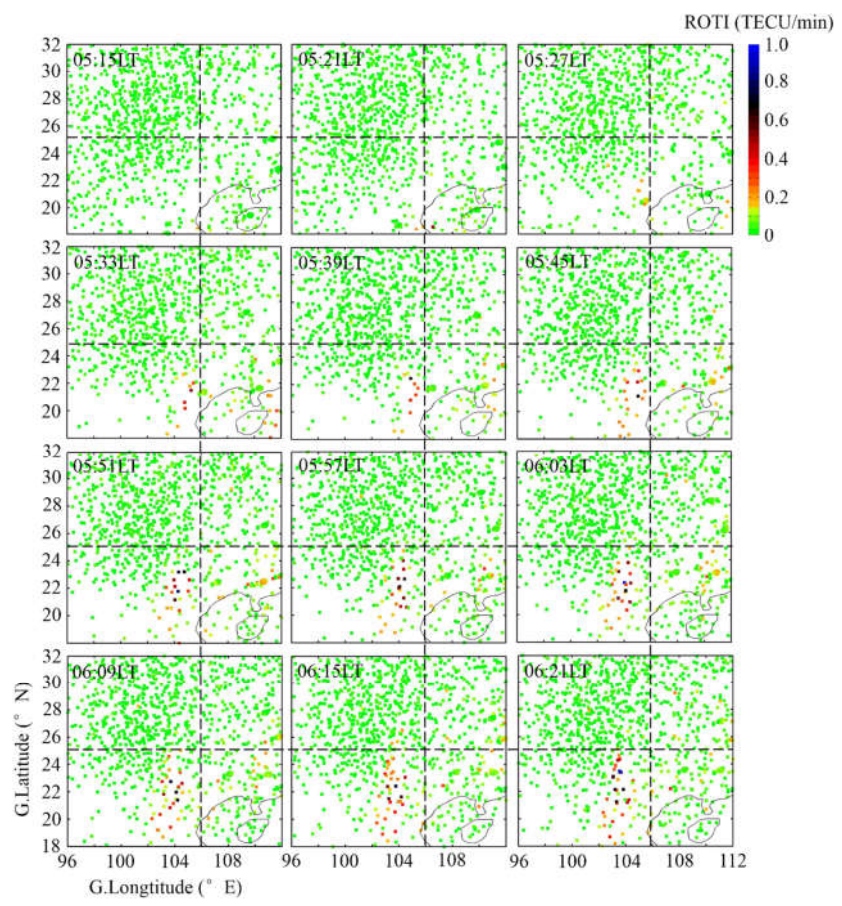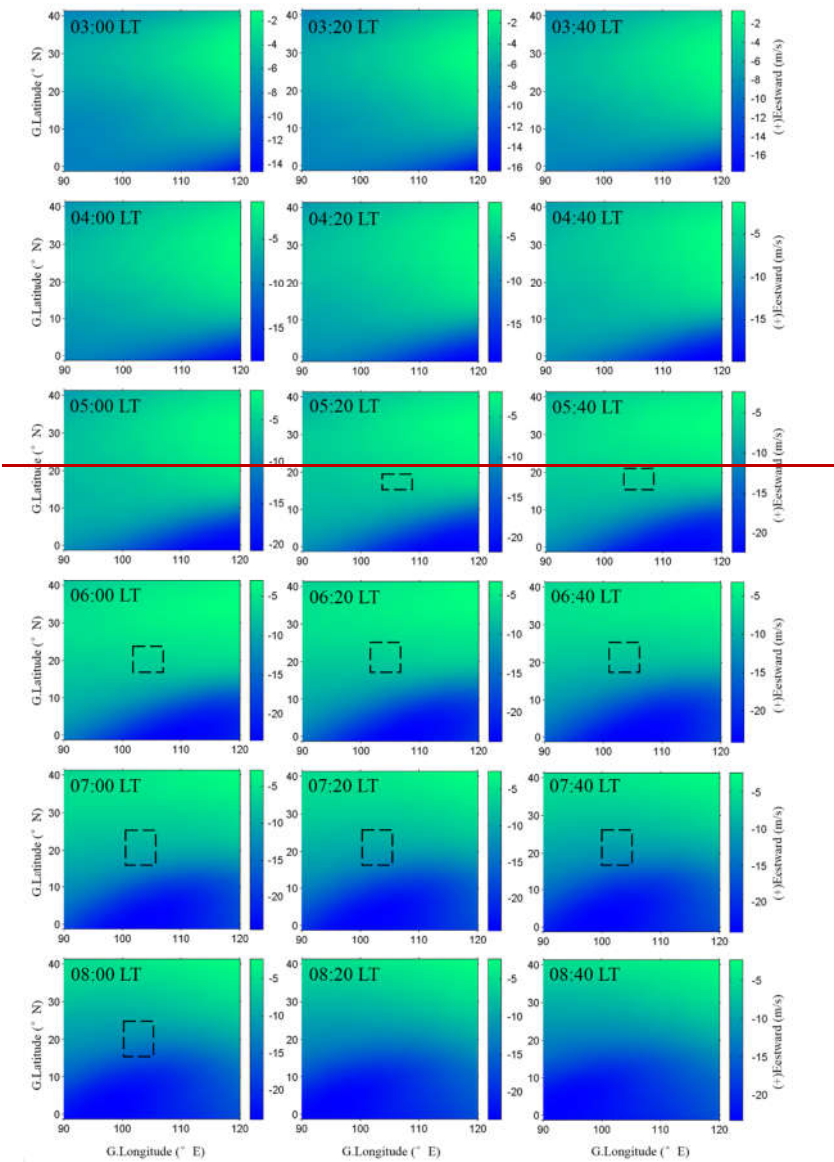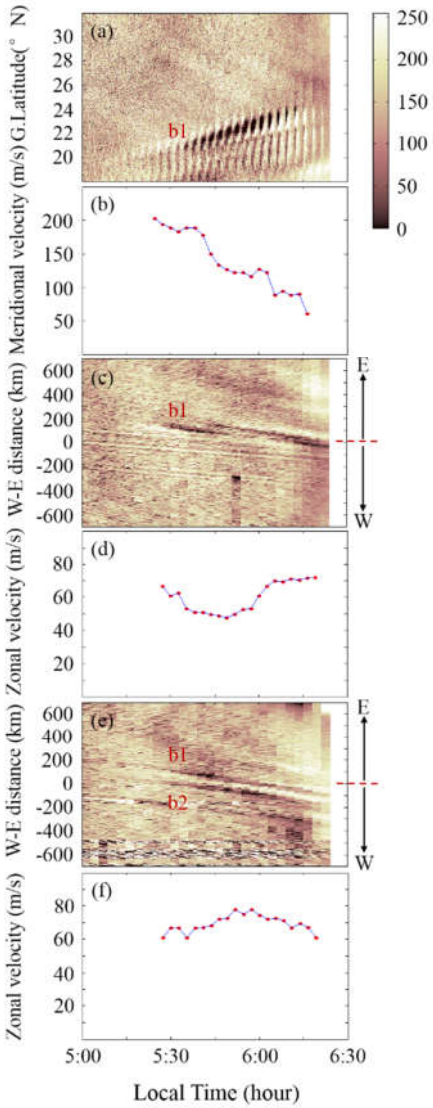
26
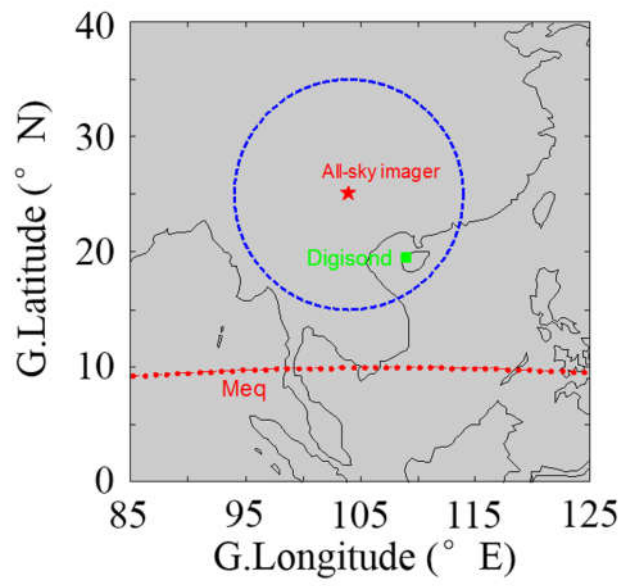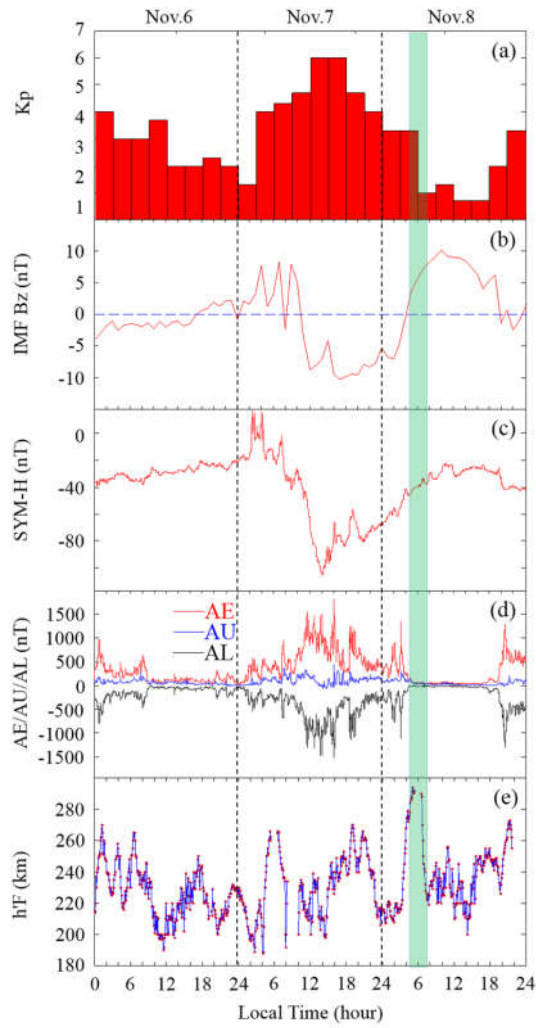
Figure 1

Figure 2

Figure 3
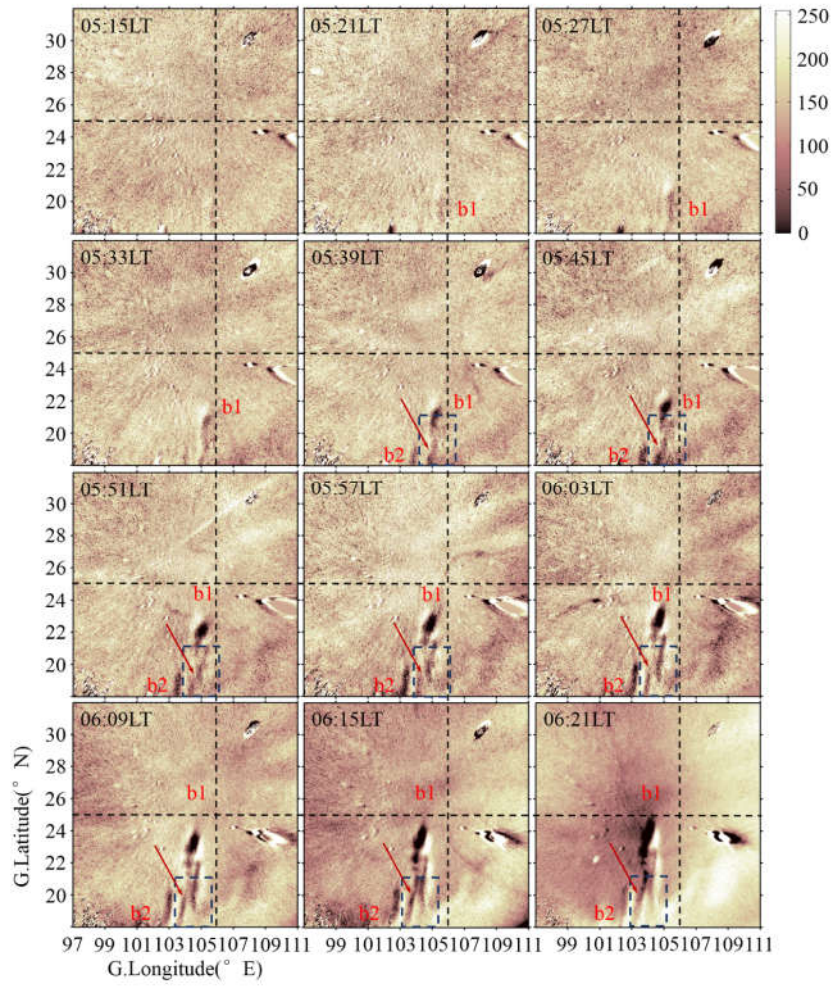
Figure 4
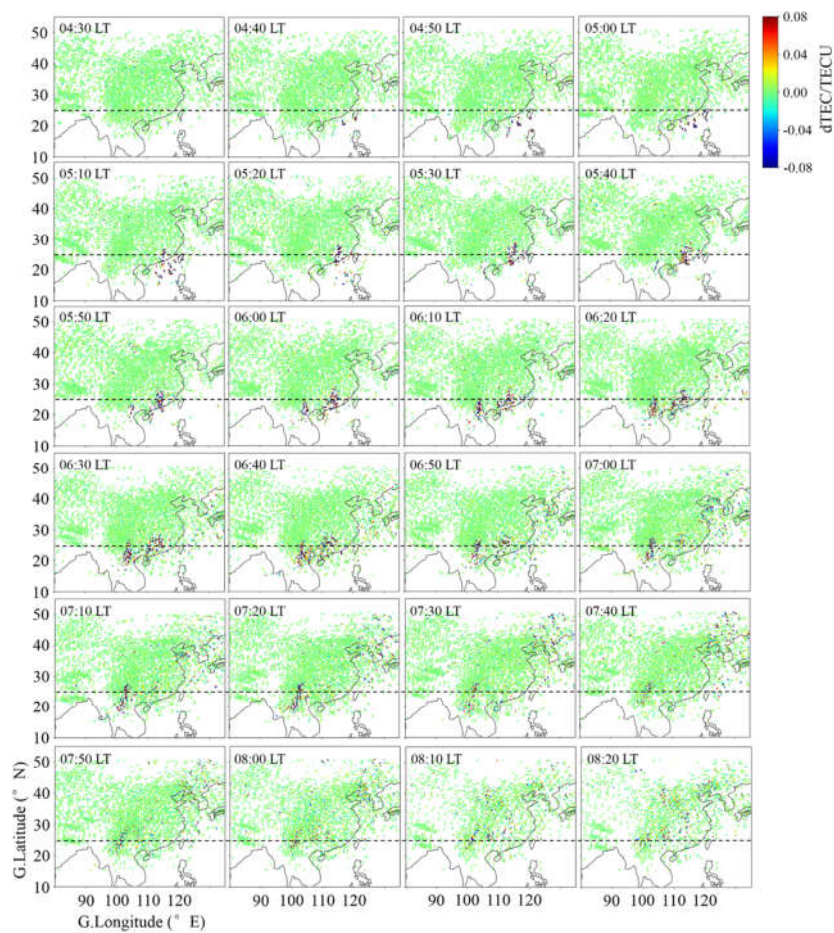
Figure 5
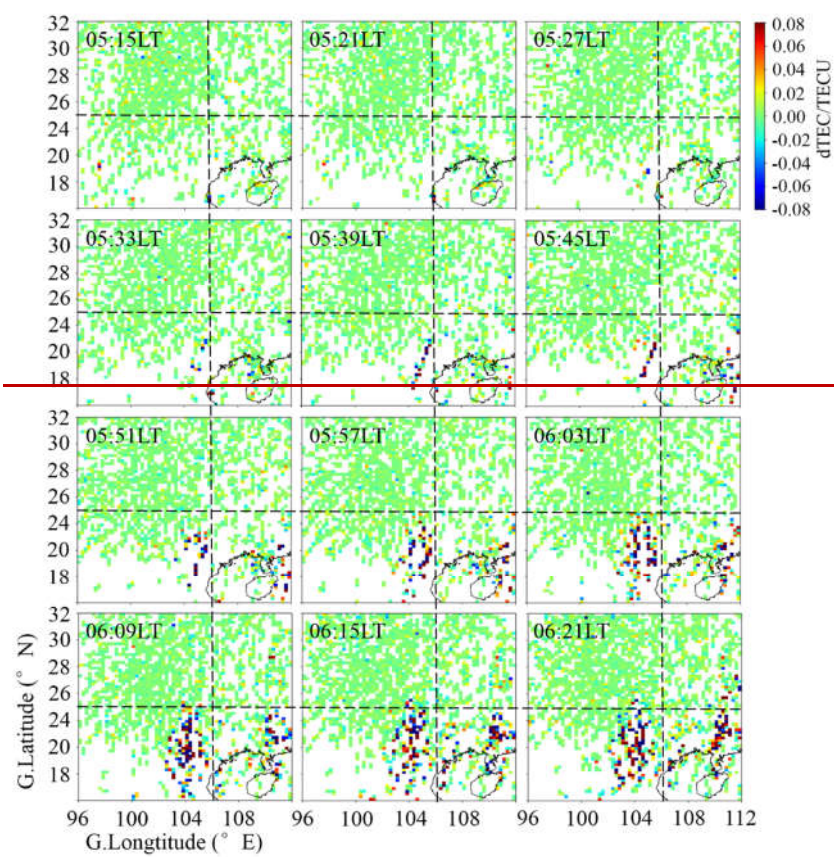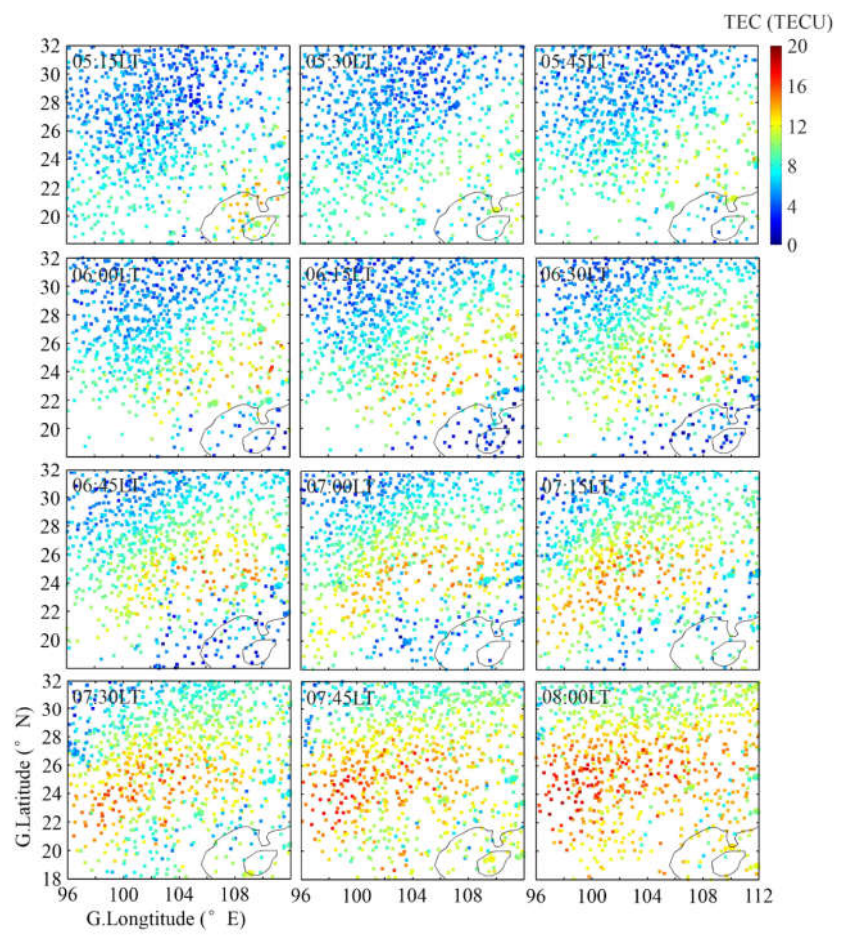
Figure 6

Figure 7

Figure 8

Figure 9

Figure 10